powders

MDPI

Article

Statistical Variability of Image-Derived Observables in Rotating-Drum Tests of a Cohesive Metal Powder: Dynamic Angle of Repose Versus Contour-Length Statistics

Jun Katagiri [1,*], Masahiro Kusano [2] and Makoto Watanabe [2]

[1] Degradation Diagnostics Research Team, Integrated Research Center for Resilient Infrastructure, National Institute of Advanced Industrial Science and Technology, Higashi 1-1-1, Tsukuba 305-8567, Ibaraki, Japan
[2] Research Center for Structural Materials, National Institute for Materials Science, Sengen 1-2-1, Tsukuba 305-0047, Ibaraki, Japan
* Correspondence: j-katagiri@aist.go.jp

Abstract

Rotating-drum tests are widely employed for the characterization of powder flowability through image-derived free-surface observables. However, the statistical stability of the selected observable is rarely examined, although it directly determines the number of images required for reliable evaluation. In the present study, two observables obtained from rotating-drum tests of a cohesive metal powder are compared: the dynamic angle of repose (AoR) and a contour-length-based index, R, derived from the extracted free-surface contour. Using identical experimental conditions and image sequences, the observables are evaluated in terms of their mean values, coefficients of variation (CVs), and the sample sizes required to achieve a prescribed relative precision. The CV of AoR ranged from 0.095 to 0.186, whereas that of R remained below 0.03. For a target relative error of 3%, the required numbers of cases were estimated to be 21, 84, and 189 for AoR at the 1σ, 2σ, and 3σ confidence levels, respectively, whereas those for R were 1, 1, and 2. These results demonstrate that, even under identical apparatus and powder conditions, the statistical burden of characterization depends strongly on observable choice. In the present study, the contour-length-based index R is interpreted as a geometry-based descriptor of free-surface irregularity rather than as a direct measure of cohesion or adhesion. Because the analysis is limited to a single cohesive metal powder, the present findings should be interpreted as a case-specific demonstration within the current experimental framework rather than as a general law for all cohesive powders.

Keywords: rotating drum; cohesive powder; dynamic angle of repose; image-derived observable; statistical variability

Check for updates

Academic Editor: Paul F. Luckham

Received: 21 May 2026
Revised: 3 July 2026
Accepted: 16 July 2026
Published: 21 July 2026

1. Introduction

Powder flowability is important in a wide range of engineering processes, including handling, filling, mixing, granulation, and additive manufacturing. Among the available experimental methods, rotating-drum tests have been widely used because they allow continuous observation of free-surface dynamics with a relatively simple apparatus configuration [1–3].

In practical applications, commercially available rotating-drum powder rheometers such as the GranuDrum and the Revolution Powder Analyzer (RPA) are also used, and image-derived angle-based and surface-shape-based observables have become established tools for powder characterization [4–7].

In such instruments, the measured quantity is not limited to a single angle-based output. Depending on the analysis logic and the built-in processing workflow, rotating-drum characterization may provide observables related to average slope, interface irregularity, or other morphology-dependent features. Some descriptors are defined internally by the instrument software, whereas others can be derived by custom image processing from the same side-view images. This means that, even when the apparatus, powder, and operating conditions are fixed, the outcome of characterization may still depend strongly on which observable is selected for analysis. From a measurement-design perspective, the choice of observable is therefore not merely a post-processing detail, but part of the experimental protocol itself.

Among image-derived observables, the dynamic angle of repose (AoR) is the most widely used and serves as a practical descriptor of flowability, internal friction, and cohesion [8–12]. For cohesive or adhesive powders, however, the free surface often fluctuates irregularly owing to localized agglomeration, intermittent collapse, and surface undulations [8,9,13–15]. Under such conditions, observables should be evaluated not only in terms of physical meaning but also in terms of how stably they can be estimated.

Even when an observable has a clear physical interpretation, large frame-to-frame variability implies that many images are required to estimate its mean reliably. Conversely, if another observable extracted from the same image sequence has substantially smaller variance, it may provide a more efficient and reproducible descriptor under the same apparatus and operating conditions. Therefore, in rotating-drum characterization, observable selection should account not only for physical interpretability but also for statistical stability, required sample size, and experimental cost.

Despite its practical importance for measurement design, previous studies have mainly focused on mean AoR values, rotation-speed dependence, hysteresis, and qualitative features of free-surface morphology [1,2,16,17]. In particular, for cohesive powders in rotating drums, irregular free surfaces and clustering have been discussed extensively, whereas direct comparisons of the statistical burden associated with different observables remain limited [13,14,16,17]. A systematic discussion of coefficients of variation and the number of cases required for statistically reliable estimation is still uncommon.

At the same time, the broader science of powder flowability characterization includes well-established shear-test-based frameworks in which bulk quantities such as yield locus, cohesion, internal friction, unconfined yield strength, and flow function are used to characterize powder behavior and its reproducibility [18,19]. Schulze's round-robin study on ring shear testers is particularly relevant because it treats not only mean shear stresses and yield loci, but also standard deviations, confidence intervals, reference ranges, and the influence of ambient conditions on reproducibility [18]. Tomasetta et al. further illustrate how annular shear-cell measurements can provide Coulomb-type descriptors such as cohesion, internal friction angle, major principal stress, unconfined yield strength, and flow factor, and can detect changes in cohesive behavior caused by temperature-dependent interparticle interactions or liquid-bridge formation [19]. In parallel, recent morphology-oriented studies have also highlighted that full-field or profile-shape information may provide complementary insight beyond single angle-based descriptors alone [20].

The relevant literature can be grouped into several partially overlapping streams. One stream focuses on classical rotating-drum or related angle-of-repose measurements, where mean values, flow regimes, or hysteresis are the main outcomes. A second stream is associated with commercial powder-rheometry tools, in which built-in image-derived descriptors, including angle-based and morphology-related indices, are used for practi-

https://doi.org/10.3390/powders5030027

cal powder characterization. A third stream addresses repeatability, reproducibility, or measurement sensitivity, often from the viewpoint of instrument performance rather than direct comparison between observables. A fourth stream examines cohesive or partially saturated granular flow, where clustering, adhesion, and irregular free-surface morphology are central issues. These studies are all relevant to the present work, but they are not usually discussed within a common framework of statistical burden and observable selection.

Table 1 summarizes representative studies relevant to rotating-drum characterization. In addition to classical angle-based measurements, the recent literature includes commercial image-derived descriptors implemented in instruments such as the GranuDrum and the Revolution Powder Analyzer, standardization efforts, and studies addressing repeatability or measurement sensitivity. However, these aspects are not always discussed together. As indicated in Table 1, previous studies have commonly emphasized mean AoR values, flow regimes, or instrument-defined descriptors. By contrast, direct comparisons of statistical burden across different observables extracted from the same image sequence remain limited. This distinction is especially important for cohesive powders, in which clustering, adhesion, and intermittent collapse may increase the frame-to-frame variability of some observables much more strongly than others.

Table 1. Representative studies relevant to rotating-drum characterization, with emphasis on observables, variability reporting, and morphology-related descriptors.

Ref.	System	Method	Observable	Variability	Morphology
[1]	Dry grains	Drum	AoR	Ltd.	No
[16]	Wet grains	Drum	AoR/flow	Partial	Qual.
[4]	Powders	GranuDrum	Drum indices	No	Yes
[5]	AM powder	RPA	AoR/fractal	No	Yes
[7]	Metal powders	Drum rheom.	R&R metrics	R&R	Built-in
[6]	Powders	GranuDrum	Flowability	Standard	Built-in
[21]	Powders	Drum tools	Sensitivity	No	Poly-fit
[22]	Metal powders	Multi-test	AoR/AIFE	No	No
[13]	Sat. grains	Drum	Flow regime	No	Qual.
[15]	Cohesive grains	Drum	Regime/size	No	Qual.
[23]	Cohesive grains	Drum	AoR/velocity	No	Qual.
[18]	Limestone powder	Ring shear	Yield locus/SD	Yes	No
[19]	Powders	Annular shear	$C/\phi/f_c/ffc$	Rep.	No

AoR, angle of repose; R&R, repeatability and reproducibility; Qual., qualitative; Ltd., limited; Sat., partially saturated; AIFE, avalanche angle/basic flowability evaluation; SD, standard deviation; Rep., repeated measurements; C, cohesion; ϕ, angle of internal friction; f_c, unconfined yield strength; ffc, flow factor.

The studies summarized above also indicate that the present work lies at the intersection of two broader streams of research. One is the established literature on bulk flowability characterization, where shear-test-based descriptors such as cohesion, internal friction, yield locus, unconfined yield strength, and flow function are used to quantify powder behavior and its reproducibility [18,19]. In that literature, the material response is obtained under prescribed consolidation and shear histories, and the scatter of the measured stresses is itself an important part of method validation [18]. The other stream is the growing recognition that morphology- or profile-based descriptors can provide complementary information beyond single angle-based metrics, especially when free-surface geometry fluctuates irregularly [20]. These broader contexts motivate the present comparison, while the scope of this study remains limited to two observables extracted from the same rotating-drum image sequence.

The scope of the present study should therefore be defined precisely. The objective is neither to replace existing instrument-defined descriptors nor to argue that a single

https://doi.org/10.3390/powders5030027

morphology-related quantity should supersede angle-based characterization in general. Rather, the present work examines whether different observables extracted from the same image sequence impose materially different statistical burdens on experimental evaluation. A direct comparison within a single apparatus, a single powder system, and a single image-analysis framework is advantageous in this respect, because it isolates the influence of observable definition from variations in hardware, operating protocol, and material class. The study is thus positioned as an examination of measurement design in rotating-drum characterization, with particular emphasis on repeatability, required sample size, and the experimental cost of obtaining statistically reliable representative values. Within this framework, the contour-length-based index R is treated as a geometry-based observable that reflects the tortuosity or morphology-related irregularity of the extracted free-surface contour. It is not introduced here as a direct measure of cohesion, powder-wall adhesion, or any other single bulk material property. Accordingly, the present results are intended as a methodological case study for the powder examined here, not as a universal characterization rule applicable to all cohesive powders.

In this study, we use the GranuDrum rotating-drum analyzer to examine a cohesive Hastelloy X metal powder. From the same image sets, we extract two observables: the dynamic angle of repose, as a representative angle-based descriptor, and a contour-length-based index R, derived from the extracted free-surface contour. We compare these observables from a statistical perspective by evaluating not only their mean values but also their standard deviations, coefficients of variation (CVs), and the number of cases required to estimate the mean at a prescribed relative precision. The purpose of this study is not to propose a new universal powder metric but rather to demonstrate how observable choice governs statistical stability and measurement burden in image-based rotating-drum characterization. Accordingly, the physical role of R is discussed in terms of the free-surface geometry that it reflects, rather than in terms of a claimed one-to-one correspondence with a specific material parameter.

2. Materials and Methods

2.1. Material

The powder used in this study was a gas-atomized Hastelloy X metal powder manufactured by Höganäs Höganäs AB, Höganäs, Skåne Län, Sweden. Hastelloy X is a Ni-based superalloy with high corrosion resistance and good high-temperature strength, and it is commonly supplied for additive manufacturing applications. The particle-size distribution of the powder was characterized by a mean particle size of 29 μm, with $D_{10} = 19$ μm and $D_{90} = 46$ μm. A nominal particle density of 8.22×10^3 kg m^{-3} was used as a material descriptor of the Hastelloy X alloy. In contrast, independent measurements of bulk density, cohesion, and powder–wall interaction parameters were not part of the present rotating-drum campaign. Accordingly, the present study does not assign separate quantitative values to those properties, and the interpretation is restricted to the image-derived observables extracted from the rotating-drum tests. The powder was stored in a laboratory environment at 20–25 °C without active humidity control.

The powder adhered weakly to the inner wall of the storage container. During the rotating-drum tests, the free surface did not remain smooth or straight but instead showed irregular temporal variations accompanied by the formation and disappearance of cohesive clusters. In this study, such behavior was regarded as being consistent with cohesive powder flow.

https://doi.org/10.3390/powders5030027

2.2. Rotating-Drum Apparatus and Protocol

Experiments were conducted using a commercially available GranuDrum Granutools SRL, Awans, Belgium. The drum is a horizontally mounted cylindrical cell with an inner diameter of 84 mm. The powder was loaded to approximately half of the drum volume, corresponding to a filling fraction of about 0.5.

The rotation speed ω was set to 2, 4, 6, 8, and 10 rpm. For each experimental series, an increasing–decreasing protocol was adopted. The drum speed was first increased stepwise from 2 to 10 rpm and then decreased stepwise from 10 to 2 rpm. Representative side-view images for the experiments are shown in Figure 1, together with typical examples of local image noise as described in the next subsection. The five values above represent distinct nominal rotation-speed setpoints. Because each setpoint was visited on both the increasing and decreasing branches, each experimental series contained ten speed–branch conditions. The protocol was a stepwise setpoint protocol rather than a continuous ramp-rate experiment; images acquired during transitions between setpoints were not used for the analysis. Instead, the side-view images used for analysis were those recorded after the flow had reached a steady state at each prescribed speed. The 2–10 rpm range was selected as a low-speed protocol that maintained a stable side-view free surface for the tested cohesive Hastelloy X powder while providing multiple regularly spaced flow conditions. The purpose of this speed selection was to compare the statistical stability of the two image-derived observables under identical operating conditions, rather than to map all possible flow regimes over the full operating range of the apparatus.

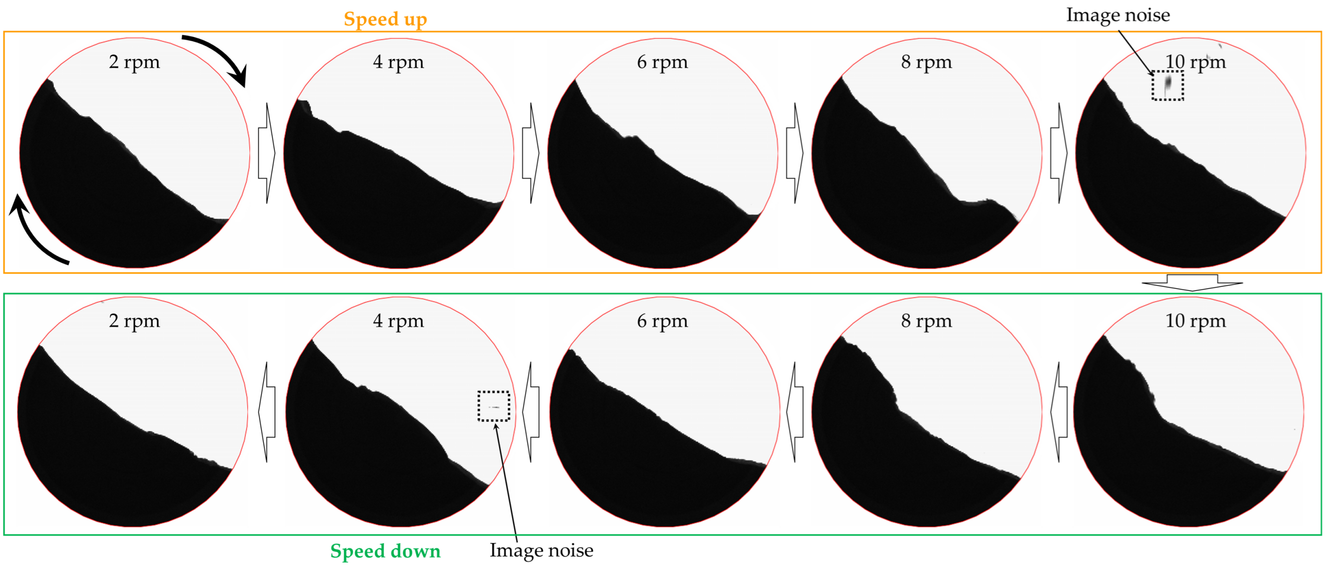

Figure 1. Representative side-view images obtained during the increasing and decreasing speed sequences in the rotating-drum tests. The upper row shows the increasing branch (2, 4, 6, 8, and 10 rpm), and the lower row shows the decreasing branch (2, 4, 6, 8, and 10 rpm). Dotted boxes indicate typical examples of local image noise caused by wall-adhered particles or isolated powder fragments.

At each speed, side-view images of the free surface were recorded after the flow had reached a steady state. For each condition, 20 images were analyzed. With three independent series, two speed branches, five rotation speeds, and 20 images per condition, the total number of analyzed images was 600.

In this study, apparatus and imaging conditions were kept as constant as possible. This design enabled a direct comparison of how differences in observable definition appear as differences in statistical variability.

https://doi.org/10.3390/powders5030027

The main powder properties and experimental conditions are summarized in Table 2. This summary distinguishes between nominal descriptors available for the tested alloy and quantities that would require separate dedicated rheological measurements.

Table 2. Powder properties and experimental conditions used in the rotating-drum tests.

Item	Value
Powder	Gas-atomized Hastelloy X
Mean particle size	29 μm
D_{10}	19 μm
D_{90}	46 μm
Nominal particle density ρ_p	8.22×10^3 kg m^{-3}
Image-derived observables	AoR and R
Independent bulk-density measurement	Not performed in the present campaign
Independent cohesion/powder–wall interaction	Not measured in the present campaign
Storage temperature	20–25 °C
Humidity control	Not controlled
Drum inner diameter D	84 mm
Filling fraction	∼0.5
Rotation speeds ω	2, 4, 6, 8, and 10 rpm
Number of nominal speed setpoints	5
Speed increment	2 rpm
Protocol	Increasing–decreasing
Speed–branch conditions per series	10
Number of series	3
Images per condition	20
Images during speed transitions	Not used for analysis
Total number of images	600

2.3. Image Processing and Definition of Observables

The acquired images were first converted to grayscale and then binarized to extract the powder region. Otsu's method [24] was used to determine the threshold automatically.

To avoid discontinuities and strong curvature near the wall boundaries, a central square analysis window of side length $0.6D$ was used for free-surface analysis because the image width of the circular drum region corresponds to the drum diameter D. Figure 2 illustrates the analysis window, the fitted angle-of-repose line, the contour-length-based index (R), and typical examples of local image noise considered in the extraction procedure.

The free-surface contour was extracted by scanning this analysis window column by column. For each column, contiguous powder regions were identified, and the uppermost pixel of each contiguous region was treated as a free-surface candidate. A continuous free-surface profile was then constructed by selecting candidate points sequentially according to vertical continuity with the neighboring column. This procedure reduced the risk of misidentifying isolated adhered particles and detached powder clusters as part of the free surface.

The dynamic angle of repose, θ, was defined as the inclination angle of the best-fit straight line to the extracted free-surface points. Because the image coordinate system is positive downward, the sign of the vertical coordinate was inverted before linear fitting.

The contour-length-based index R was defined from the same free-surface point set. The polyline length of the extracted free surface, L_{surface}, was calculated and normalized by the straight-line distance between the two endpoints of the contour, L_{chord}:

$$R = \frac{L_{\text{surface}}}{L_{\text{chord}}}.$$

https://doi.org/10.3390/powders5030027

For a nearly straight free surface, $R \approx 1$. As the free surface becomes more tortuous, L_{surface} increases and R becomes larger. In this study, R is therefore interpreted as a geometry-based descriptor of the irregularity or tortuosity of the extracted free surface. Because it is derived solely from the contour shape, R should not be interpreted as a direct measure of cohesion, adhesion, or other single material properties. Instead, it provides a complementary observable that is sensitive to the morphology of the free surface under the present rotating-drum conditions.

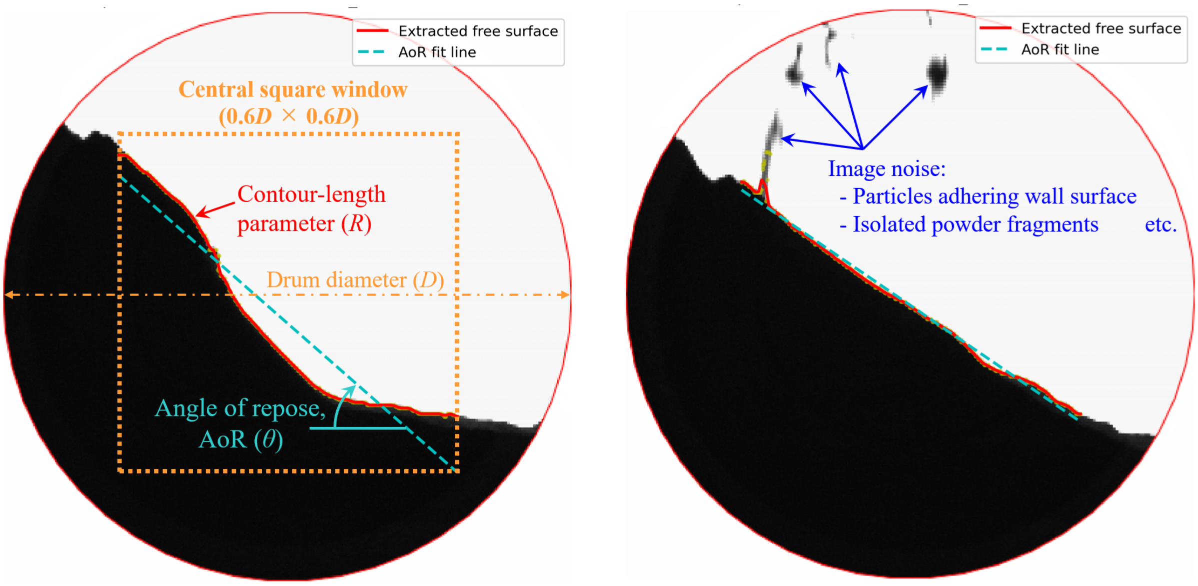

Figure 2. Definition of the image-based observables and examples of local image noise. The upper panel illustrates a central square analysis window of side length $0.6D$, where D denotes the drum diameter and corresponds to the image width of the circular drum region, together with the extracted free-surface contour, the fitted line for the dynamic angle of repose (AoR), and the contour-length-based index R. The lower panel shows typical local image noise, such as wall-adhered particles and isolated powder fragments.

The images may contain local noise caused by powder particles adhering to the wall or by isolated powder fragments (see Figures 1 and 2). Such noise may artificially extend the extracted free-surface contour and can result in overestimation of the contour length and instability in slope estimation. In the present study, only the uppermost pixel of each contiguous powder region in a given column was regarded as a free-surface candidate, and the final candidate was selected according to continuity with neighboring columns. As illustrated in Figure 2, this procedure mitigated the influence of such noise on the extracted free surface. Although the present extraction logic reduces the impact of image noise, some sensitivity to image-processing parameters is nevertheless expected. A systematic assessment of this sensitivity is left for future work.

2.4. Statistical Analysis

For each condition (series, branch, and rotation speed), the instantaneous values of θ and R were obtained from individual images. From these values, the mean, standard deviation, and coefficient of variation (CV) were calculated. The CVs were defined as

$$CV_\theta = \frac{\sigma_\theta}{\bar{\theta}}, \qquad CV_R = \frac{\sigma_R}{\bar{R}},$$

where $\bar{\theta}$ and $\bar{R}$ are the mean values of θ and R, and σ_θ and σ_R are their corresponding standard deviations.

To quantify the sampling burden, the minimum number of cases required to estimate a mean value within a prescribed relative error ε was evaluated using the normal approximation:

$$n \geq \left(\frac{z\,CV}{\varepsilon}\right)^2,$$

where z is the standard normal quantile corresponding to the confidence level. In this study, $\varepsilon = 0.03$ was used, and the required number of cases was evaluated for 68.3% (1σ), 95.4% (2σ), and 99.7% (3σ) confidence levels.

2.5. Temporal Dependence Assessment

Because the image-by-image measurements were obtained from continuous rotating-drum sequences, the possible temporal dependence between successive observations was examined additionally. For each condition (series, branch, and rotation speed), lag-k sample autocorrelation coefficients were calculated separately for the dynamic angle of repose (θ) and the contour-length-based index (R) using the image order within the analyzed sequence:

$$\rho_k = \frac{\sum_{t=1}^{N-k}(x_t - \bar{x})(x_{t+k} - \bar{x})}{\sum_{t=1}^{N}(x_t - \bar{x})^2},$$

where x_t denotes the observable at image index t, $\bar{x}$ is its sample mean, and N is the number of analyzed images for the condition. In the present study, $N = 20$ for each condition. The purpose of this supplementary analysis was not to establish an exact stochastic model for the free-surface dynamics, but to assess whether strong serial dependence was present to an extent that would substantially affect the interpretation of the sample-size estimates. Because the image acquisition interval was not available from the outsourced experimental procedure, the autocorrelation analysis was used as an empirical diagnostic rather than as a strict proof of independence. Accordingly, the required numbers of cases reported in this study should be interpreted primarily as comparative indicators of relative statistical burden within the present experimental framework.

3. Results

3.1. Representative Images and Extracted Free Surfaces

Within the analysis window shown in Figure 2, the free surface was tracked continuously from left to right, and both AoR and R were computed from the same set of extracted free-surface points. The differences between AoR and R, as discussed below, can therefore be attributed to differences in the definition of the observable rather than to variations in image input or apparatus conditions.

3.2. Mean Values of AoR and R

Figure 3 shows the mean values of AoR and R as functions of rotation speed ω. The upper panel shows the mean AoR, whereas the lower panel shows the mean contour-length-based index R. The mean AoR, $\bar{\theta}$, ranged approximately from 33 to 39°, with an overall mean of 35.4°. The mean contour-length-based index, $\bar{R}$, ranged from 1.028 to 1.056, with an overall mean of 1.041. Neither observable showed a strong systematic trend over the tested speed range, although R remained confined to a narrower range than AoR.

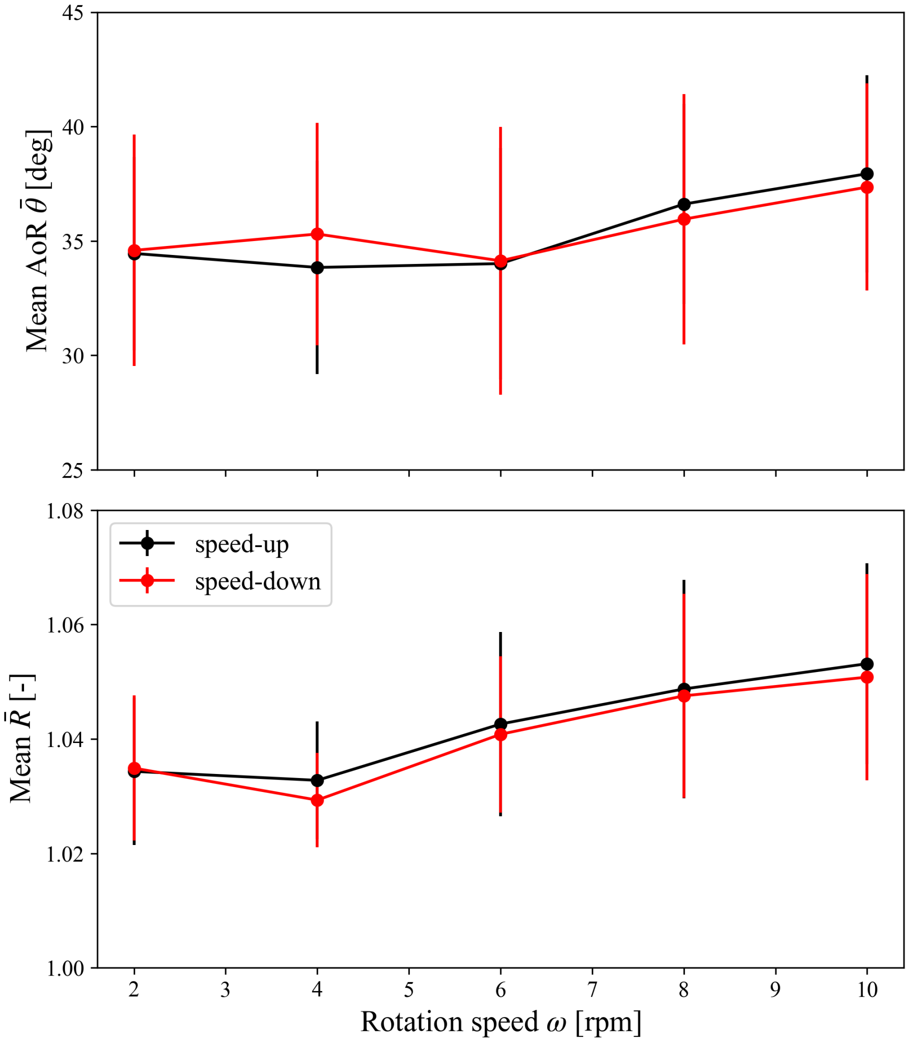

Figure 3. Mean values of the two image-derived observables as functions of rotation speed ω. The upper panel shows the mean dynamic angle of repose, $\bar{\theta}$, and the lower panel shows the mean contour-length-based index, $\bar{R}$. Black and red symbols denote the increasing (speed-up) and decreasing (speed-down) branches, respectively. Error bars indicate the standard deviations calculated from the image-by-image measurements.

3.3. Comparison of Variability: AoR Versus R

Figure 4 compares the coefficients of variation of AoR and R on the same axis. The CV of AoR ranged from 0.095 to 0.186, with an overall mean of 0.137. In contrast, the CV of R ranged from 0.0069 to 0.027, with an overall mean of 0.014. Thus, even though the two observables were extracted from the same image sets, the relative variability of AoR was approximately one order of magnitude larger than that of R.

AoR is the slope of a fitted straight line and is therefore sensitive to local surface undulations and small collapse events. By contrast, R represents the total length of the free surface and effectively integrates local fluctuations over the entire contour. For this reason, R tends to show smaller relative variability.

https://doi.org/10.3390/powders5030027

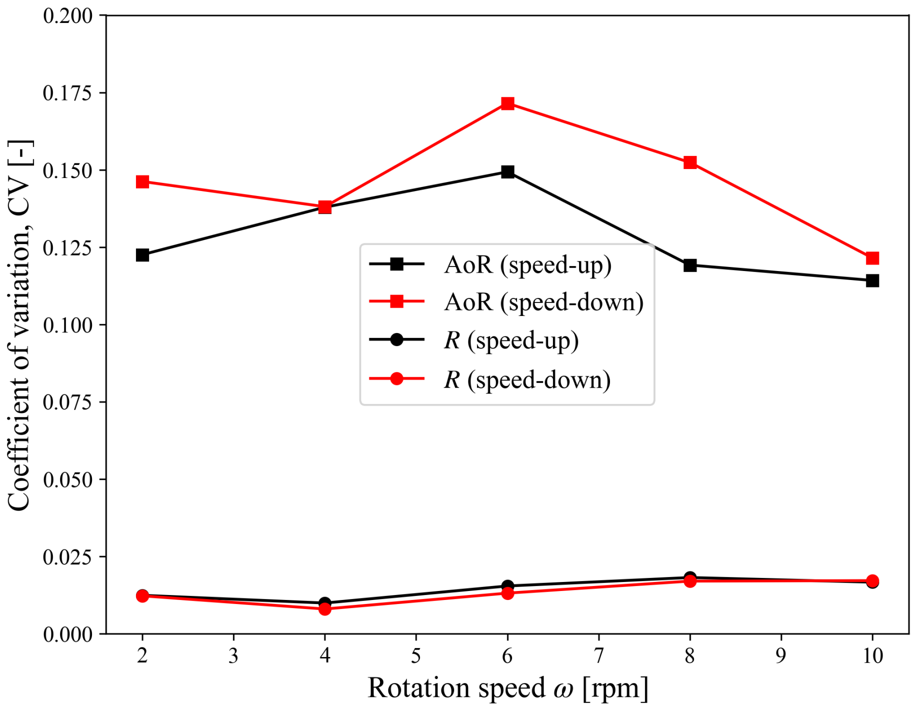

Figure 4. Direct comparison of the coefficients of variation (CVs) of the dynamic angle of repose (AoR) and the contour-length-based index R as functions of rotation speed ω. Black and red symbols denote the increasing (speed-up) and decreasing (speed-down) branches, respectively. Square markers correspond to AoR, and circular markers correspond to R.

3.4. Required Number of Cases

As suggested by the large difference in CV shown in Figure 4, the sampling burden differed markedly between the two observables. Table 3 summarizes the required numbers of cases for a target relative error of 3% at three confidence levels. The difference in CV directly appears as a difference in the number of cases required for reliable mean estimation. For AoR, the required numbers of cases were 21, 84, and 189 for 1σ, 2σ, and 3σ, respectively. For R, the corresponding numbers were 1, 1, and 2.

Table 3. Required numbers of cases for estimating the mean values of AoR and R within a relative error of 3% at three confidence levels.

Confidence Level	z	**AoR**	$\boldsymbol{R}$
68.3% (1σ)	1	21	1
95.4% (2σ)	2	84	1
99.7% (3σ)	3	189	2

These results indicate that, even under identical apparatus, powder, and operating conditions, the experimental burden required to obtain a statistically reliable representative value depends strongly on which observable is selected.

3.5. Autocorrelation Analysis

Figure 5 summarizes the lag-1 autocorrelation coefficients of θ and R for each rotation speed and branch. For both observables, the lag-1 autocorrelation coefficients were generally close to zero and showed no systematic positive trend across the tested speeds. Averaged over all 30 conditions, the lag-1 autocorrelation coefficient was -0.093 for θ and -0.116 for R.

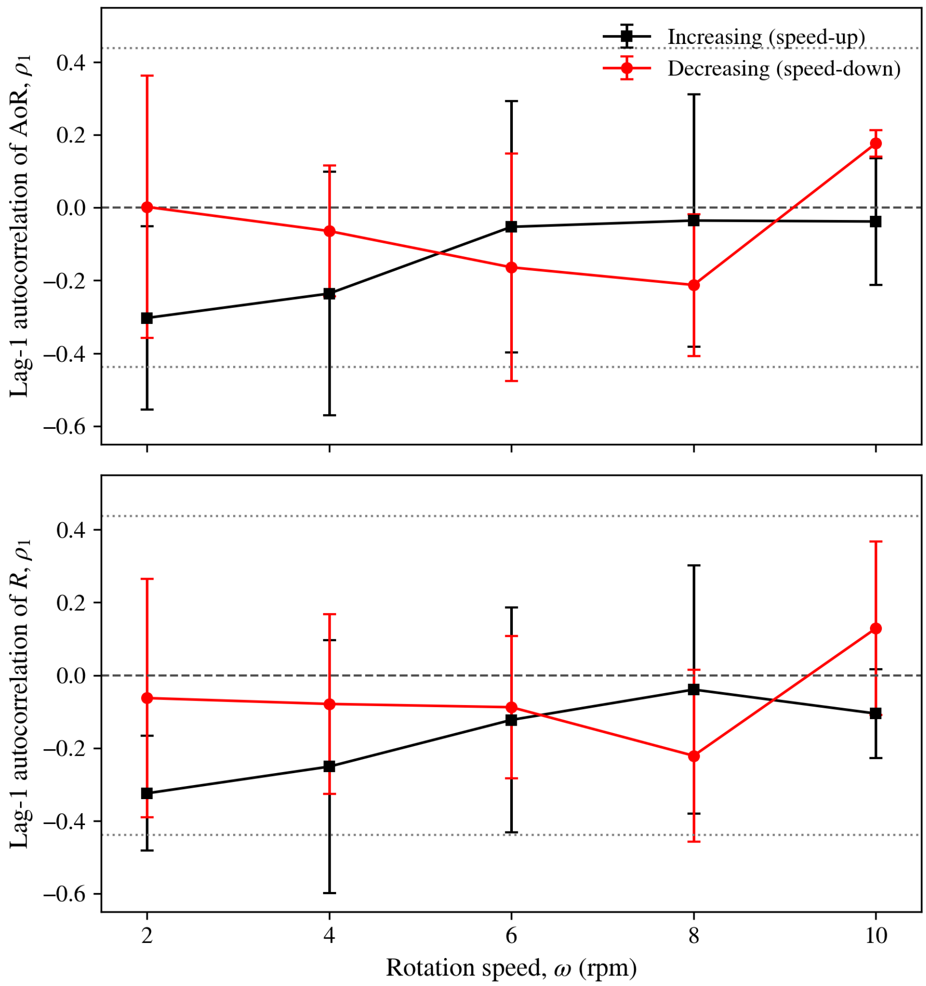

Figure 5. Lag-1 autocorrelation coefficients of the dynamic angle of repose (AoR) and the contour-length-based index R as functions of rotation speed ω. The upper panel shows AoR and the lower panel shows R. Black and red symbols denote the increasing (speed-up) and decreasing (speed-down) branches, respectively. Each point represents the mean over the three repeated series, and the error bars denote the standard deviation. The horizontal dashed line indicates $\rho_1 = 0$, and the dotted lines indicate the approximate white-noise reference bounds, $\pm 1.96/\sqrt{20}$.

Using the approximate white-noise reference bound $\pm 1.96/\sqrt{20}$, only 4 of 30 conditions for θ and 4 of 30 conditions for R exceeded this range in absolute value, and all of these cases corresponded to negative rather than positive lag-1 autocorrelation. These results suggest that, for the present image sets, the observed contrast in statistical burden between θ and R is unlikely to be explained primarily by strong positive frame-to-frame correlation. Accordingly, the required numbers of cases reported in Table 3 remain useful as approximate comparative indicators of relative sampling burden. At the same time, because the measurements were extracted from continuous image sequences and the image acquisition interval was not available from the outsourced experimental procedure, the sample-size estimates should not be interpreted as universally transferable exact requirements.

4. Discussion

4.1. Why Do AoR and R Impose Different Statistical Burdens?

The difference in statistical stability between AoR and R can be understood directly from their definitions. AoR is the inclination of a fitted straight line and therefore responds directly to local changes in the free-surface geometry. In cohesive powder flow, localized cluster formation and intermittent collapse can perturb the fitted slope significantly, leading to relatively large frame-to-frame fluctuations in AoR.

By contrast, R is based on the total contour length normalized by the chord length. Local roughness events do contribute to L_{surface}, but their effects are distributed over the whole contour. As a result, R is less sensitive to local surface events and tends to remain statistically more stable. At the same time, this statistical stability should not be taken to mean that R is universally more physically informative than AoR. Rather, the two observables emphasize different aspects of the same free surface: AoR is more directly related to the mean inclination, whereas R reflects contour irregularity distributed over the analyzed interface.

4.2. Relationship to Established Powder Flowability Characterization and Implications for Image-Based Observables

The connection with established powder flowability characterization is important, but it should be interpreted carefully. In ring shear or annular shear tests, the powder is subjected to prescribed normal stresses and shear histories, and the resulting yield loci are used to derive bulk material descriptors such as cohesion, internal friction angle, unconfined yield strength, and flow function [18,19]. Schulze's round-robin test also shows that reproducibility is evaluated through the scatter of measured shear stresses and that ambient conditions such as humidity can contribute to the observed standard deviation [18]. Tomasetta et al. show that annular shear-cell measurements can detect changes in cohesive behavior when interparticle interactions change, for example through temperature-dependent liquid-bridge formation [19].

An important point is that this study does not claim to introduce a fundamentally new roughness metric. Nor does it claim that R is a direct surrogate for cohesion, adhesion, internal friction, unconfined yield strength, or flow factor. The practical relevance of R in the present work lies in the fact that it captures morphology-related irregularity of the free surface while requiring a much smaller sampling burden under otherwise identical imaging conditions. For example, the GranuDrum itself provides an automated roughness-related index, and previous studies have already recognized the importance of free-surface length and contour geometry in rotating-drum characterization [3,5,6,23]. At the same time, the broader powder-characterization literature includes established shear-test-based descriptors such as yield locus, cohesion, internal friction angle, unconfined yield strength, and flow function, as well as recent arguments that morphology-based information may complement angle-based metrics [18–20]. The present rotating-drum observables are therefore best regarded as image-derived descriptors that are complementary to conventional bulk flowability measurements, rather than as substitutes for them. However, although previous studies have reported that cohesion can increase variability in angle-based measurements, systematic discussions of statistical accuracy, such as comparisons of CV and required sample size across different observables, remain limited [13,14,16,17].

The key contribution of the present study is to show that, even within a single experiment, the reliability of measured values depends strongly on observable choice. As a consequence, the number of cases required to obtain a statistically reliable representative value can change by more than an order of magnitude. In this sense, the present work should be viewed not as a proposal of a replacement for AoR, but as an experimental demonstration that observable choice governs measurement burden in image-based rotating-drum characterization. The statistical stability of an observable and its physical relevance should therefore be discussed separately: the former determines how efficiently a representative value can be estimated, whereas the latter depends on which feature of the free-surface dynamics the observable is designed to reflect. Because only one cohesive metal powder was examined, the magnitude of the difference observed here between AoR

https://doi.org/10.3390/powders5030027

and R should not be assumed to be universally transferable across powder classes, particle morphologies, or cohesion levels.

A further implication of the present results concerns DEM parameter calibration. The angle of repose has long been used as a convenient macroscopic target for DEM calibration because of its experimental simplicity. However, recent inverse-analysis work has shown that calibration based solely on the angle of repose can become ill-conditioned, and that observational variability in AoR may strongly amplify the uncertainty of calibrated parameters, particularly those associated with rolling resistance [25]. From this perspective, the present result is relevant: the contour-length-based index R exhibited substantially smaller CV and a much lower sampling burden than AoR under the same experimental conditions. This suggests that low-variability observables such as R, when combined with AoR, may provide a more stable experimental basis for future multi-objective DEM calibration. At present, however, this study does not perform such calibration explicitly, and the extent to which R improves parameter identifiability should be examined in future work. The additional autocorrelation analysis showed no systematic positive serial dependence in either observable sequence. Therefore, the large contrast in required sample size between AoR and R is unlikely to be explained solely by temporal persistence in the image acquisition order, although the reported sample-size values should still be interpreted as approximate comparative indicators within the present framework.

4.3. Limitations

This study has several limitations that should be acknowledged. First, only one cohesive metal powder was examined, and generalization to non-cohesive powders or powders with varying degrees of cohesion requires further investigation. Accordingly, the present study should be interpreted as a methodological case study rather than as a cross-material validation. In addition, the tested rotation-speed range was limited to 2–10 rpm; therefore, the conclusions should not be extrapolated to higher-speed regimes or to other operating protocols without additional validation. Second, the analysis was based on two-dimensional side-view images and did not address possible three-dimensional free-surface effects. Third, the contour-length-based index R is a deliberately simple geometrical quantity, and comparison with other roughness metrics or multiscale descriptors remains a subject for future work. Likewise, its relationship to independent measurements of cohesion, adhesion, or bulk flowability has not been established in the present study and should be examined separately in future work. Because independent ring-shear, annular-shear, wall-friction, compression, or other powder-rheometry measurements were not performed in the present campaign, no quantitative correlation can be established here between R and conventional flowability descriptors such as yield locus, cohesion, internal friction angle, unconfined yield strength, flow function, compressibility, or stress-relaxation parameters. Cross-material validation, including powders with different morphologies and cohesion levels and comparison with independent shear-cell or powder-rheometer measurements, remains an important subject for future work. Finally, because the image acquisition interval was not available from the outsourced experimental procedure, temporal dependence could only be assessed indirectly from the observable sequences themselves. Although the additional autocorrelation analysis did not indicate systematic positive serial dependence, the sample-size estimates reported here should still be regarded as approximate comparative indicators rather than exact universal requirements.

5. Conclusions

In this study, a commercially available GranuDrum was used to evaluate the statistical stability of two image-derived observables for a cohesive Hastelloy X metal powder: the dynamic angle of repose (AoR) and a contour-length-based index R. The main findings can be summarized as follows.

1. An improved free-surface extraction procedure enabled stable tracking of the free surface within the central square analysis window of side length $0.6D$.
2. The coefficient of variation of AoR ranged from 0.095 to 0.186, with an average of 0.137, whereas the coefficient of variation of R ranged from 0.0069 to 0.027, with an average of 0.014. Thus, R showed approximately one order of magnitude smaller relative variability than AoR.
3. For a target relative error of 3%, the required numbers of cases for AoR were 21, 84, and 189 at the 1σ, 2σ, and 3σ confidence levels, respectively, whereas those for R were 1, 1, and 2. The additional autocorrelation analysis showed no systematic positive lag-1 serial dependence in either observable sequence, supporting the use of these values as approximate comparative indicators of relative sampling burden.
4. These results demonstrate that, in rotating-drum image analysis, observable choice strongly affects statistical stability and measurement efficiency. Within the present framework, R should be interpreted as a geometry-based descriptor of free-surface irregularity, not as a direct measure of cohesion or adhesion.

Overall, these results indicate that image-based characterization of cohesive powder flow should consider not only the physical meaning of an observable but also its statistical stability and sampling burden. For the cohesive Hastelloy X powder examined here, this point is established as a case-specific experimental result within the present rotating-drum image-analysis framework.

Author Contributions: Conceptualization, J.K.; methodology, J.K.; software, J.K.; validation, J.K.; formal analysis, J.K., M.K. and M.W.; investigation, J.K.; resources, J.K.; data curation, J.K.; writing—original draft preparation, J.K. and M.K.; writing—review and editing, J.K., M.K. and M.W.; visualization, J.K. All authors have read and agreed to the published version of the manuscript.

Funding: This research received no external funding.

Data Availability Statement: The processed data and analysis scripts supporting the findings of this study are available from the corresponding author upon reasonable request. The raw image data are not publicly available at this stage because they have not yet been prepared for public deposition.

Conflicts of Interest: The authors declare no conflicts of interest.

Abbreviations

The following abbreviations are used in this manuscript:

AM	Additive manufacturing
AoR	Angle of repose
CV	Coefficient of variation
DEM	Discrete element method
Qual.	Qualitative
R&R	Repeatability and reproducibility
RPA	Revolution Powder Analyzer

References

1. Liu, X.Y.; Specht, E.; Mellmann, J. Experimental study of the lower and upper angles of repose of granular materials in rotating drums. *Powder Technol.* **2005**, *154*, 125–131. [CrossRef]
2. Liu, X.Y.; Zhang, Y.Y. Real-time detection of the repose angle of solids in rotating drum based on image processing. *Adv. Mater. Res.* **2011**, *301–303*, 748–751. [CrossRef]
3. Taberlet, N.; Richard, P.; Hinch, E.J. S shape of a granular pile in a rotating drum. *Phys. Rev. E* **2006**, *73*, 050301. [CrossRef]

4. Neveu, A.; Francqui, F.; Lumay, G. Measuring powder flow properties in a rotating drum. *Measurement* **2022**, *200*, 111548. [CrossRef]
5. Pleass, C.; Jothi, S. Influence of powder characteristics and additive manufacturing process parameters on the microstructure and mechanical behaviour of Inconel 625 fabricated by Selective Laser Melting. *Addit. Manuf.* **2018**, *24*, 419–431. [CrossRef]
6. *ASTM D8648-25*; Standard Test Method for Determining Flowability Using GranuDrum. ASTM International: West Conshohocken, PA, USA, 2025.
7. Tondare, V.N.; Whiting, J.G.; Pintar, A.L.; Moylan, S.P.; Neveu, A.; Francqui, F. An interlaboratory study for assessing repeatability and reproducibility of the data generated by rotating drum powder rheometers (Part 1: Granudrum). *Powder Technol.* **2024**, *441*, 119810. [CrossRef]
8. Herminghaus, S. Dynamics of wet granular matter. *Adv. Phys.* **2005**, *54*, 221–261. [CrossRef]
9. Mitarai, N.; Nakanishi, H. Wet granular materials. *Adv. Phys.* **2006**, *55*, 1–45. [CrossRef]
10. Elekes, F.; Parteli, E.J.R. An expression for the angle of repose of dry cohesive granular materials on earth and in planetary environments. *Proc. Natl. Acad. Sci. USA* **2021**, *118*, e2107965118. [CrossRef]
11. Müller, D.; Fimbinger, E.; Brand, C. Algorithm for the determination of the angle of repose in bulk material analysis. *Powder Technol.* **2021**, *383*, 598–605. [CrossRef]
12. Geldart, D.; Abdullah, E.C.; Verlinden, A. Characterisation of dry powders. *Powder Technol.* **2009**, *190*, 70–74. [CrossRef]
13. Dong, M.; Wang, Z.; Marks, B.; Chen, Y.; Gan, Y. Partially saturated granular flow in a rotating drum: The role of cohesion. *Phys. Fluids* **2023**, *35*, 113302. [CrossRef]
14. Samadani, A.; Kudrolli, A. Angle of repose and segregation in cohesive granular matter. *Phys. Rev. E* **2001**, *64*, 051301. [CrossRef]
15. Pol, A.; Artoni, R.; Richard, P. Cohesive granular material in a rotating drum: Flow regimes and size effects. *J. Fluid Mech.* **2025**, *1006*, A24. [CrossRef]
16. Chou, S.H.; Hsiau, S.S. Experimental analysis of the dynamic properties of wet granular matter in a rotating drum. *Powder Technol.* **2011**, *214*, 491–499. [CrossRef]
17. Wang, W.; Barés, J.; Renouf, M.; Azéma, E. Flow regimes and repose angle in a rotating drum filled with highly concave particles. *Phys. Rev. E* **2025**, *112*, 015417. [CrossRef] [PubMed]
18. Schulze, D. Round robin test on ring shear testers. *Adv. Powder Technol.* **2011**, *22*, 197–202. [CrossRef]
19. Tomasetta, I.; Barletta, D.; Poletto, M. The High Temperature Annular Shear Cell: A modified ring shear tester to measure the flow properties of powders at high temperature. *Adv. Powder Technol.* **2013**, *24*, 609–617. [CrossRef]
20. Gaboriault, O.; Succar, A.; Delétre, C.; Timercan, A.; Pelletier, R.; Melancon, D.; Blais, B. From Angle of Repose to Heap Morphology: Full-Field Calibration of DEM for Granular Powders. *arXiv* **2026**, arXiv:2605.09371. [CrossRef]
21. Jenkins, B.D.; Nicuşan, A.L.; Neveu, A.; Lumay, G.; Francqui, F.; Seville, J.P.K.; Weston, D.; Werner, D.; Windows-Yule, C.R.K. The sensitivity of powder characterization tool measurements to particle properties. *Powder Technol.* **2024**, *448*, 120231. [CrossRef]
22. Zegzulka, J.; Gelnar, D.; Jezerská, L.; Prokeš, R.; Rozbroj, J. Characterization and flowability methods for metal powders. *Sci. Rep.* **2020**, *10*, 21004. [CrossRef] [PubMed]
23. Brewster, R.; Grest, G.S.; Levine, A.J. Effects of cohesion on the surface angle and velocity profiles of granular material in a rotating drum. *Phys. Rev. E* **2009**, *79*, 011305. [CrossRef] [PubMed]
24. Otsu, N. A Threshold Selection Method from Gray-Level Histograms. *IEEE Trans. Syst. Man Cybern.* **1979**, *9*, 62–66. [CrossRef]
25. Katagiri, J.; Shoji, N.; Yoneda, J.; Takeya, S. Limits of identifiability and uncertainty propagation in DEM parameter calibration using the angle of repose as the objective function. *Comput. Part. Mech.* **2026**, *14*, 334–345. [CrossRef]